materials

MDPI

Article

Investigation and Optimization of the C-ANN Structure in Predicting the Compressive Strength of Foamed Concrete

Dong Van Dao [1,*], Hai-Bang Ly [1], Huong-Lan Thi Vu [1], Tien-Thinh Le [2,*] and Binh Thai Pham [1]

[1] University of Transport Technology, Hanoi 100000, Vietnam; banglh@utt.edu.vn (H.-B.L.); lanvth@utt.edu.vn (H.-L.T.V.); binhpt@utt.edu.vn (B.T.P.)

[2] Institute of Research and Development, Duy Tan University, Da Nang 550000, Vietnam

* Correspondence: dongdv@utt.edu.vn (D.V.D.); letienthinh@duytan.edu.vn (T.-T.L.)

Received: 31 December 2019; Accepted: 27 February 2020; Published: 28 February 2020

Abstract: Development of Foamed Concrete (FC) and incessant increases in fabrication technology have paved the way for many promising civil engineering applications. Nevertheless, the design of FC requires a large number of experiments to determine the appropriate Compressive Strength (CS). Employment of machine learning algorithms to take advantage of the existing experiments database has been attempted, but model performance can still be improved. In this study, the performance of an Artificial Neural Network (ANN) was fully analyzed to predict the 28 days CS of FC. Monte Carlo simulations (MCS) were used to statistically analyze the convergence of the modeled results under the effect of random sampling strategies and the network structures selected. Various statistical measures such as Coefficient of Determination (R^2), Mean Absolute Error (MAE), and Root Mean Squared Error (RMSE) were used for validation of model performance. The results show that ANN is a highly efficient predictor of the CS of FC, achieving a maximum R^2 value of 0.976 on the training part and an R^2 of 0.972 on the testing part, using the optimized C-ANN-[3–4–5–1] structure, which compares with previous published studies. In addition, a sensitivity analysis using Partial Dependence Plots (PDP) over 1000 MCS was also performed to interpret the relationship between the input parameters and 28 days CS of FC. Dry density was found as the variable with the highest impact to predict the CS of FC. The results presented could facilitate and enhance the use of C-ANN in other civil engineering-related problems.

Keywords: Compressive Strength; Foamed Concrete; Artificial Neural Network; Monte Carlo simulations

1. Introduction

Over the past decades, large-scale, super-tall, or mega-tall buildings have been increasingly constructed over the world [1,2]. This fact raises a number of fundamental engineering problems, crucial to be solved, such as self-weight, large foundation sizes, and earthquake resistance [3,4]. Apart from the structural problems, the weight of conventional concrete is also a major drawback from a material point of view [5]. Foamed Concrete (FC) appears as a potential replacement of conventional concrete to be used in specific engineering applications. Since the early 1920s, when the Swedish architect Johan Eriksson was granted the patent on FC, many further inventions have been developed and applied in practice by experts in America, Japan, and Europe [6]. Lightweight concrete, known as cellular concrete or FC, is a recently developed concrete with many advantages [7,8]. Cellular concrete is made by generating air bubbles in the cement paste or mortar. These bubbles have diameters ranging from 0.1 to 1 mm [9,10] and air is usually contained within 50% of the volume [11]. The presence of

bubbles reduces the specific gravity of FC to between 400 and 1600 kg/m^3 [3,12,13]. Many researches have pointed out that the outstanding advantages of FC is lightweight, thermal insulation, sound insulation, and void filling [6,11]. Moreover, FC can be produced at low cost, it is easy to construct, and benefits from being a low waste, eco-friendly material [14]. Therefore, the use of FC is increasing in the construction industry [3], for example, as thermal insulation materials for walls, sound barriers, fire walls or backfill structures, foundations, and panels for construction [11]. Furthermore, FC's low elastic modulus also eases its use in roads and tunnels, for instance, embedding of large diameter pipelines as roadbed or cushion materials to homogeneously disperse the stress from external loadings [6]. On the contrary, several problems still exist that require further investigations, which can be listed as poor stability, low strength, higher shrinkage, easy cracking, and water absorption. In particular, the Compressive Strength (CS) of FC is often low and it is often difficult to reach 25 MPa in certain cases [12,15]. The CS of FC also depends on the composition or mixture from the constituents. These points limit the application of FC in structural engineering [16,17]. As a consequence, assessing the CS of FC is crucial and becoming an essential task for researchers.

In the literature, various approaches to forecast the CS of FC have been investigated [3,6,8–10,12,14–17]. Numerous studies have also reported that the composition of the substances structure and their proportions greatly affect the CS of FC [18–20]. For example, in the work of Asadzadeh and Khoshbayan [21], to optimize various types of concrete characteristics, design-of-experiments-based statistical methods have been utilized. Response Surface Methodology (RSM) and design-expert technology have been used to create a relationship between the input factors and the mechanical responses of fly-ash lightweight concrete [22]. However, for the crushing intensity, with a standard deviation of 3.99, the coefficient of determination (R^2) is only achieved at an R^2 of 0.60. In different approaches proposed by Bing et al. [23] or Liu et al. [24], the experimental studies have been carried out with a number of 16 different types of FC, with 21 cubes of 100 mm and prisms of 100x100x515 mm^3 casted and used to investigate the development of CS over time, as well as the effect of foam volume content [23]. Regardless of these efforts, the experimental cost and time consumption are major obstacles of this approach. On the other hand, empirical equations using experimental data could be an alternative approach to estimate the CS of FC. Nevertheless, the range of input conditions is the main reason limiting the predicted CS of FC using these equations [25]. In addition, such semi-analytical equations require several constants that are not easy to obtain and highly depend on the complex relationships between the mixture constituents and the CS of FC [18–20,25,26]. Therefore, the development of an advanced numerical tool for prediction of the CS of FC is essential.

Over the past decades, machine learning (ML) models as a brand of artificial intelligence (AI) techniques have been widely used in civil engineering. Many complex problems related to structural engineering [27–29], material sciences [30–33], geotechnical engineering [34–39], and earth sciences [40–46] have been successfully resolved. The prediction of the mechanical properties of FC has also been the subject of many studies in the literature. In the work of Nguyen et al. [25], a deep neural network (DNN) model has been used to predict the CS of FC. The authors collected 177 experimental results available in the literature and obtained satisfactory correlation results with the predicted output of DNN. Besides, the gene expression programming (GEP) algorithm, an extension of the genetic algorithm (GA) and genetic programming (GP), has been applied in the work of Kiani et al. [9]. In particular, it is impossible not to mention the work of Abd et al. [47] when using Support Vector Machines (SVM) applied to 150 results from laboratory experiments. SVM using a radial basis function was proven more accurate than other functions and traditional regression functions [47]. Besides, various ML algorithms (MLR, ANN, SVR, MARS, and MARS–WCA) have been used to predict the CS of FC at different testing ages [26]. It is thus confirmed that ML algorithms are powerful numerical tools that can account for complex relationships between mixture components and help in optimizing the mixture to achieve the targeted mechanical properties, such as the CS of FC.

In this study, the performance of a Conventional Artificial Neural Network (C-ANN) algorithm was investigated to predict the 28 days CS of FC. Although ANN is one of the most effective ML

algorithms, its performance depends significantly on the selection of network structure. Thus, this study also focuses on the investigation and optimization of the C-ANN structure for better prediction of the CS of FC. To achieve this goal, previously published experimental data in the literature were gathered and randomly divided into two subsets: the training dataset (70% of data) and the testing part (30% of data). Monte Carlo simulations (MCS) were used to verify the convergence of the modeled results. In addition, Partial Dependence Plots (PDP) over 1000 MCS were also produced to interpret the relationship between input parameters and 28-day CS of FC. Various statistical measures such as Coefficient of Determination (R^2), Mean Absolute Error (MAE), and Root Mean Squared Error (RMSE) were used for validation of model performance.

2. Statement of the Novelty and Significance

The 28-days CS of FC is a key value in structural engineering, controlling the quality of construction works. While various surrogate, optimized, and hybrid ML algorithms have been used, it has been proven that a C-ANN model could still accurately predict the 28-days CS of FS, which depends significantly on the selection of the appropriate network structure. Limited efforts to find out a suitable C-ANN structure have been reported in the literature [48,49], but no systematic study has accounted for random sampling of the dataset. Therefore, the current study contributes to fill these research gaps through the following points: (i) an improved prediction of the CS of FC was achieved using C-ANN algorithm; (ii) MCS was used, for the first time, to determine the most effective C-ANN structure in the presence of random dataset splitting; (iii) a comparison with existing published results was conducted to confirm the accuracy of C-ANN; (iv) a sensitivity analysis was performed using PDP to reveal the relationships between the input variables and the 28-days CS of FC; and (v) three equations aiming to interpret the dependence of the 28-days CS of FC on dry density, water-to-cement, and sand-to-cement ratios were derived from PDP investigation.

3. Materials and Methods

3.1. Data Used

In this study, 220 data points of experiments on FC collected from the literature (Table 1) were used, including dry density (D), water/cement ratio (W/C), and sand/cement ratio (S/C) as input variables, and the CS at 28 days as an output variable. Table 1 summarizes the information of the literature constituting the database, including the number of data points collected. Besides, a summary of the statistical analysis of the three inputs and the CS as output of this study is presented in Table 2. The distribution histograms of dry density (D), water/cement ratio (W/C), sand/cement ratio (S/C), and the CS is displayed in Figure 1.

Table 1. Database collected in this study.

References	No. of Samples	Proportion (%)
Abd et al. (2017) [47]	144	65.45
Asadzadeh and Khoshbayan (2018) [21]	24	10.91
Hilal et al. (2015) [3]	7	3.18
Jones and McCarthy (2005) [12]	12	5.45
Kozłowski et al. (2015) [17]	4	1.82
Mounanga et al. (2008) [16]	4	1.82
Richard and Ramli (2013) [50]	1	0.45
Pan et al. (2007) [6]	12	5.45
Tam et al. (1987) [10]	9	4.09
Tikalsky et al. (2004) [11]	3	1.38
Total	**220**	**100**

Table 2. Statistical analysis of the data used in this study.

	Dry Density	Water/Cement	Sand/Cement	Compressive Strength (28 days)
Notation	D	W/C	S/C	CS
Unit	(kg/m^3)	-	-	(MPa)
Role	Input	Input	Input	Output
Min	430.00	0.26	0.00	0.60
Average	1566.33	0.44	1.20	22.94
Median	1639.50	0.40	1.00	24.50
Max	2009.48	0.83	4.29	48.88
SD	369.49	0.12	0.67	13.42
CV (%)	23.59	0.28	0.56	0.59

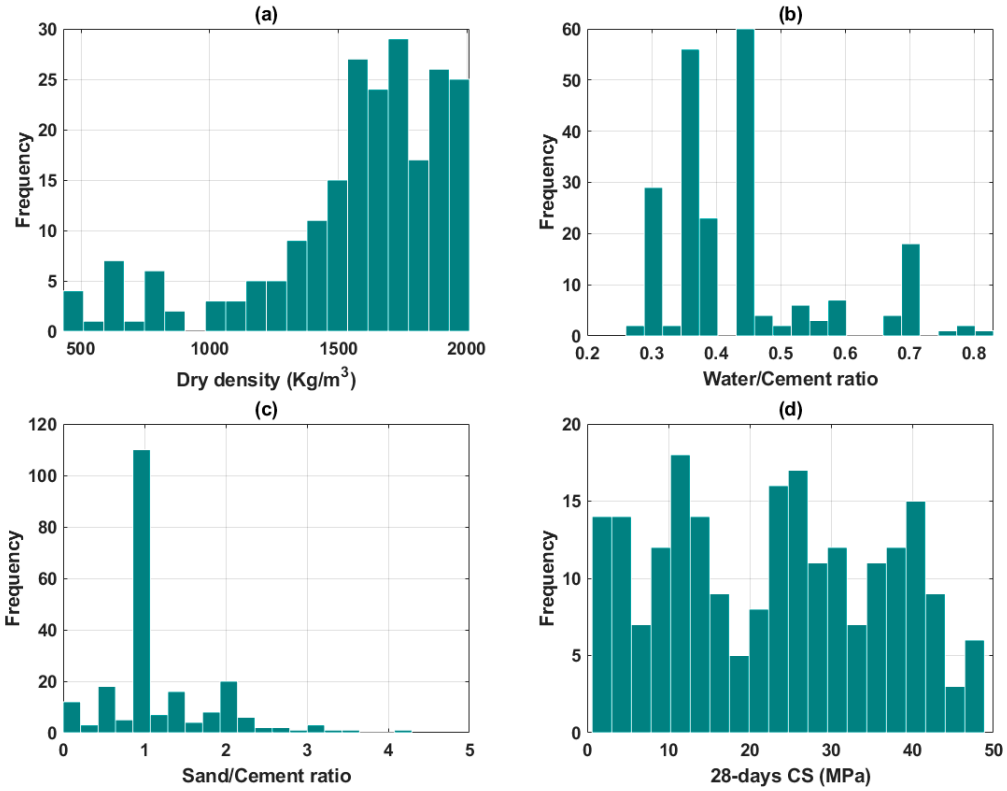

Figure 1. Distribution histograms of (**a**) dry density; (**b**) water/cement ratio; (**c**) sand/cement ratio, and (**d**) 28-days Compressive Strength (CS) of Foamed Concrete (FC).

3.2. Methods Used

3.2.1. Conventional Artificial Neural Network (C-ANN)

In the past decades, along with the intense development of computer science, AI techniques have been used to a greater extent in various areas of expertise [51]. C-ANN is the most common AI algorithm used in scientific research, especially in civil engineering [52]. C-ANN is an information processing computing system designed based on the operation of the human brain [35,53–56]. The very first study of ANN was proposed by McCulloch and Pitts [57] in the early 1940s. In fact, C-ANN is made up of multiple nodes and links that bind these nodes, and a weight which is capable of learning is associated with each link. They learn by changing the value of the weights. The training algorithm's objective is to reduce the mean square error (MSE) between the target and the predicted outputs.

The advantages of C-ANN could be various but the most important point of ANN comes from the ability to handle highly nonlinear problems [58]. Thus, complex interactions, relationships between inputs and outputs, can be modeled without knowing the correlation between these variables [58]. Thanks to

these advantages C-ANN is applied in many different fields, such as basic sciences, construction, health, and environment. The implementations of C-ANN in civil engineering are promising and many important results have been achieved over the past years [52]. In the study of Nehdi et al. [59], C-ANN was used to predict the cellular concrete output. The investigation results show that compared to existing parametric methods, C-ANN can much more accurately predict several properties of concrete, such as production yield, foamed density, un-foamed density, and the CS of cellular concrete mixtures. In another study, from 150 empirical results, Paulson et al. [60] used C-ANN to conduct a comprehensive survey to optimize the level of cement replacement with silica fume. This study pointed out that it was expected that CS and the values were similar to the experimental results, so it concluded that instead of conducting experiments, C-ANN can be used to predict the CS for various values of input [60].

3.2.2. Quality Assessment of Results

In the present study, the coefficient of determination (R^2), Mean Absolute Error (MAE), and Root Mean Squared Error (RMSE) are used as measures to evaluate the developed ML algorithms. Precisely, R^2 values allow to identify the statistical relationship between the experimental results and predicted values. It yields a value between 0 and 1, where 0 is no correlation and 1 is total correlation [61]. In the cases of RMSE and MAE, which have the same units as the quantity being estimated, lower values of RMSE and MAE basically indicate a high accuracy of prediction output using the ML models [29,32,62,63]. Values of R, RMSE, and MAE are estimated using the following equations [31,61,64,65]:

$$\mathrm{MAE} = \frac{\sum_{i=1}^{n}\left|p_i - v_i\right|}{n} \tag{1}$$

$$\mathrm{RMSE} = \sqrt{\sum_{i=1}^{n}\frac{(p_i - v_i)^2}{n}} \tag{2}$$

$$\mathrm{R}^2 = \frac{\sum_{i=1}^{n}(p_i - q)(v_i - \underline{v})}{\sqrt{\sum_{i=1}^{n}(p_i - q)^2 \sum_{i=1}^{n}(v_i - \underline{v})^2}} \tag{3}$$

where n is defined as the number of input data, p_i and v_i denoted the actual and predicted CS values, respectively, and $\underline{v}$ is the mean value of the predicted CS by C-ANN.

3.2.3. Monte Carlo Simulations (MCS)

The performance of any ML algorithm is highly depended on the way that the training dataset is constructed—that is, the data sampling method. Data sampling is a kind of statistical method used to select observations from the database whose main objective is to investigate a selected parameter. In applied machine learning, data sampling is usually referred to as the propagation of variability of inputs on the predicted output. The real performance of ML algorithms could only be accepted only if the prediction errors are low even with the presence of variability in the dataset. In order to generate such variability, MCS is used in this study. The Monte Carlo method is one of the well-known techniques to propagate input variability on the output results [63,66–69]. The Monte Carlo method is notably powerful and efficient for evaluating the performance of ML models [34,70]. Moreover, Monte Carlo allows massively parallel computing to be conducted, making it an effective strategy to reduce simulation time [71–74]. The main idea of the MCS is to use random sampling to generate as many realizations as possible in the input space. The next step is dedicated to the calculation of the output through ML models [75,76]. Finally, the obtained results of performance could be assessed using several statistical criteria. In this work, the statistical convergence of MCS is examined using the equation as follows [62,70,77,78]:

$$f_M(M) = \frac{1}{\underline{K}}\frac{1}{M}\sum_{i=1}^{M} K_i, \tag{4}$$

where $\underline{K}$ is the mean value of the considered random variable K and M is the number of Monte Carlo runs. This convergence function provides efficient information related to the computational time, reliable results for further statistical analysis.

3.3. Methodological flow chart

The methodology flowchart of the present study included five main steps, as follows:

Step 1: Preparation and pre-processing of the database, including 220 data units collected from the available literature. The three input variables were dry density, water-to-cement, and sand-to-cement ratios, and the output was the CS of FC. The histograms of the distribution of the inputs and outputs were next presented. Before further processing, the database was scaled in the (0,1) range to reduce numerical bias, as in common ML problems.

Step 2: To analyze the convergence of the C-ANN under random sampling, a number of 1000 of simulations was conducted for each combination of C-ANN. The number of neurons in the first hidden layer of the C-ANN structure was varied from 1 to 20, whereas those of the second hidden layer ranged from 0 to 20. The value of 0 is denoted with the case using only one hidden layer. A total of 420 structures was constructed using one and two hidden layers, making a total of 420,000 simulations (21 neurons in the first hidden layer x 20 neurons in the second hidden layer x 1000 simulations). It is worth noting that the exact values of the error criteria are not presented in this step. It is dedicated only for the convergence analysis of the two typical C-ANN structures.

Step 3: To determine the optimized structure of C-ANN, various structures of C-ANN were developed and validated using R^2, RMSE, and MAE. The optimized C-ANN structure was selected based on the maximum values of R^2 and minimum values of RMSE and MAE.

Step 4: Using the optimal C-ANN structure, a detailed analysis of robustness of C-ANN algorithm was carried out and presented.

Step 5: Interpretation of the relationship and dependence of the 28-days CS with the input factors (dry density, water/cement ratio, and sand/cement ratio) using C-ANN was presented using PDP.

4. Results

4.1. Convergence of C-ANN under Random Sampling Effect

Convergence of C-ANN under the random sampling effect was analyzed with a total of 420,000 simulations for 420 C-ANN structure cases. However, the convergence results of only two typical C-ANN structures (C-ANN-[3–1–1–1] and C-ANN-[3–20–20–1]) are presented in Figure 2; other cases are not shown. It is observed that the number of 1000 simulations were satisfactory for both the training and testing datasets for each case (Figure 2). With respect to the values of R^2 using C-ANN-[3–1–1–1], a fluctuation of 1% around the mean value was reached from 100 simulations (Figure 2a), whereas with the same number of runs, RMSE and MAE fluctuated around 4% of the average values (Figure 2b,c). The predicted results stabilized around the mean values (green discontinuous lines) when the number of MCS was 700. The standard deviation error of R^2, RMSE, and MAE exhibited similar trends, but getting close to the average values at 700 runs. Considering the structure C-ANN-[3–20–20–1] with the results plotted in Figure 3, the fluctuation in terms of R^2 seemed more important than the previous case, i.e., from 70% to 110% compared with a range of 90% to 105%. The 1% level of fluctuation was reached from above 800 simulations, compared with 100 runs in the previous case. An identical number of simulations was also required for the case of RMSE and MAE, as well as a more important fluctuation that was observed in contrast with the C-ANN-[3–1–1–1] structure. Nevertheless, the standard deviation of the three error criteria converged toward a value at about 500 runs (Figure 3d,e,f), smaller than the results obtained by C-ANN-[3–1–1–1].

It can be observed that the two extracted typical C-ANN structures converged toward the statistical results. Thus, all the remaining C-ANN structures, with the number of neurons in the two hidden

layers varied from 1 to 20, could also converge toward the simulation results. Thus, it can be stated that the C-ANN converged under the random sampling effect of the data used in this study.

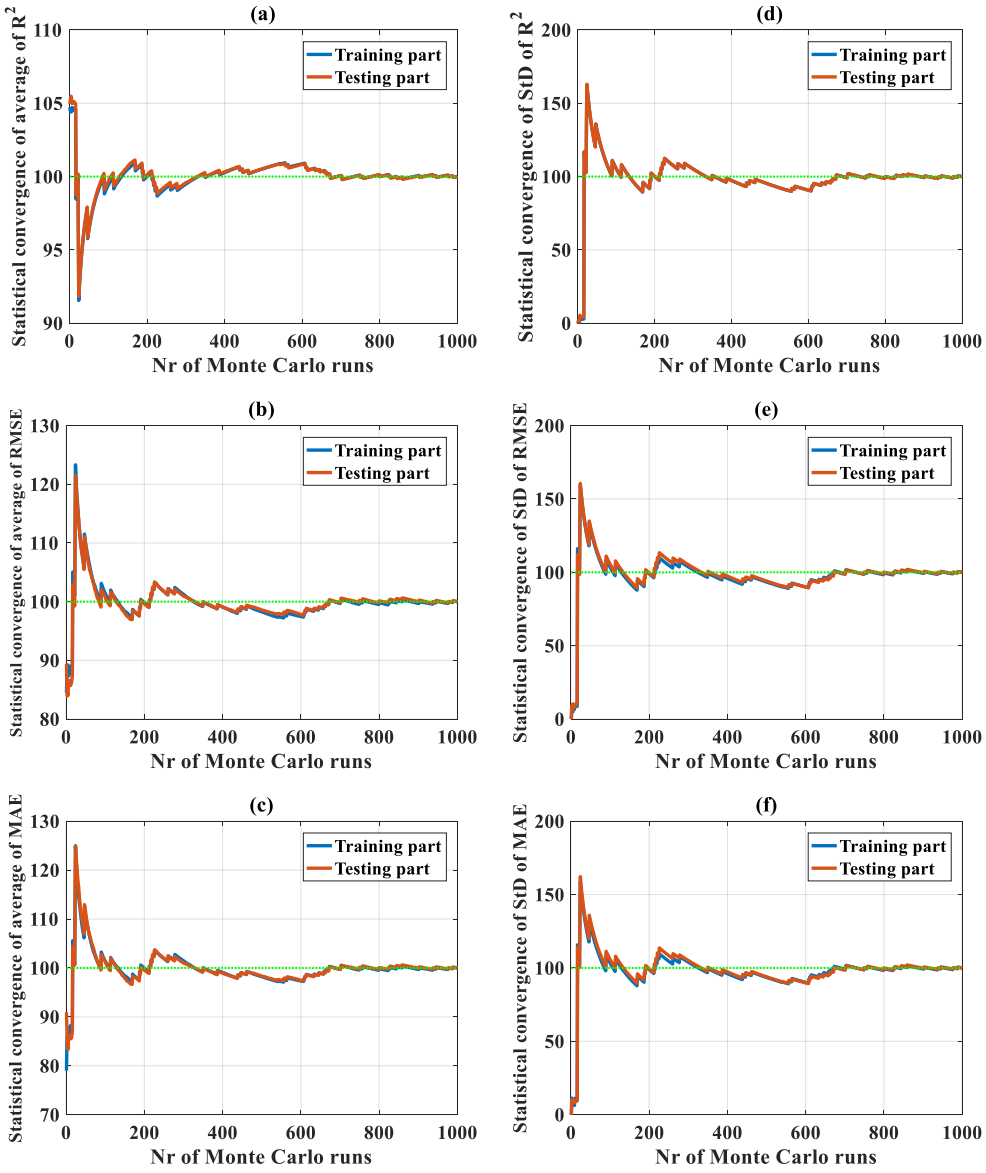

Figure 2. Convergence of random sampling in the case of using C-ANN-[3–1–1–1] for the average values of (**a**) R2, (**b**) RMSE, and (**c**) MAE; for the standard deviation (SD) values of (**d**) R^2, (**e**) RMSE, and (**f**) MAE.

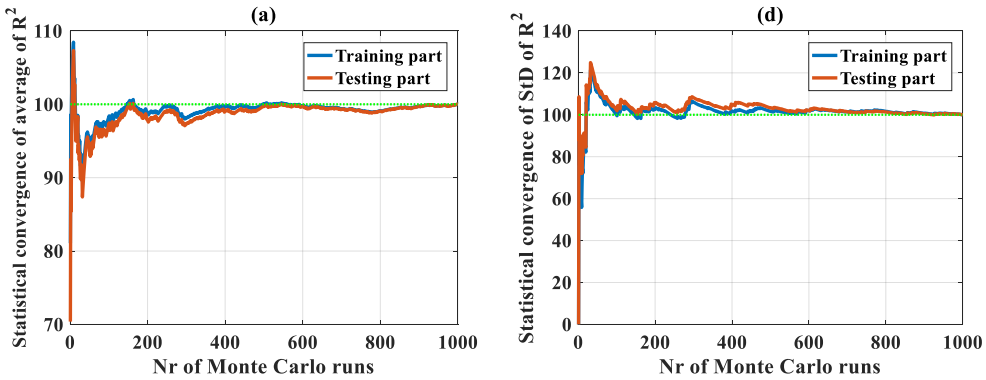

Figure 3. *Cont.*

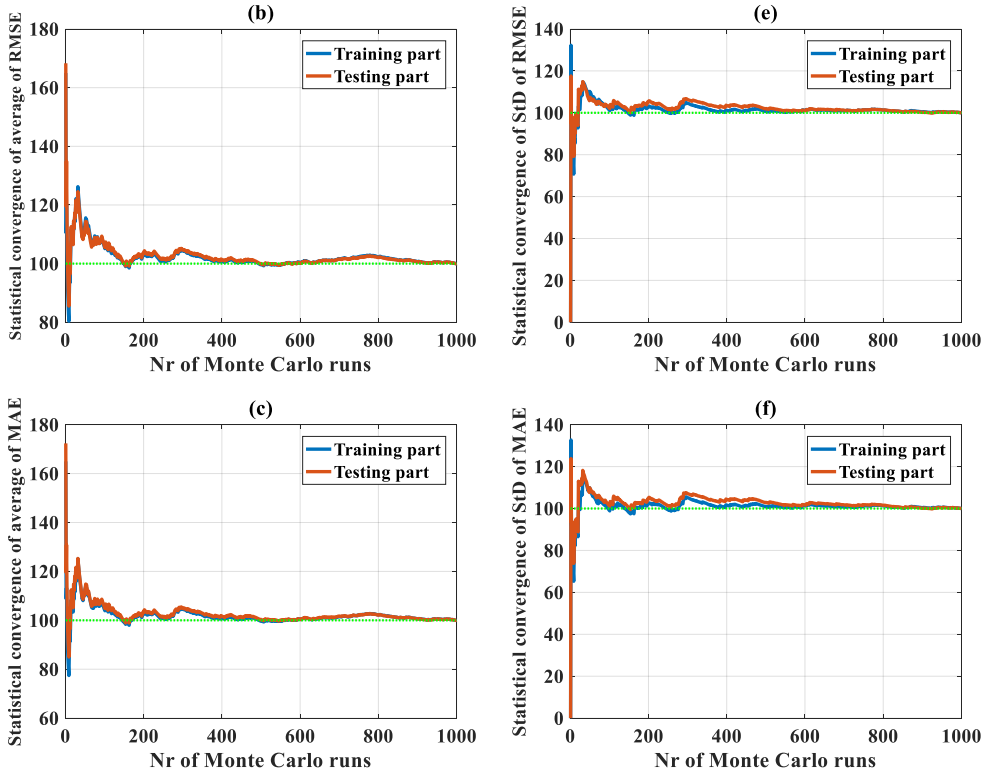

Figure 3. Convergence of random sampling in the case of using C-ANN-[3–20–20–1] for the average values of (**a**) R2, (**b**) RMSE, and (**c**) MAE; for the standard deviation (SD) values of (**d**) R^2, (**e**) RMSE, and (**f**) MAE.

4.2. Optimization of C-ANN Architecture

Various structures of C-ANN were investigated, as shown in Figure 4, for both the training and testing datasets. With respect to the training dataset, it was observed that higher number of neurons in both hidden layers produced a higher accuracy ($R^2 > 0.95$). Differently, an optimal zone was detected to achieve the highest accuracy (R^2 around 0.95) for the testing dataset (Figure 4c). This is an excellent example to demonstrate that an appropriate ANN structure must be determined before performing ML simulations. To further investigate the effect of neurons in the two hidden layers, standard deviation plots of the R^2 is presented (Figure 4b,d). The training part exhibited a small standard deviation, in general, with a low number of neurons in the second hidden layer (i.e., from 4 to 8 neurons). On the other hand, an optimal zone was observed for values of standard deviation of R^2 for the testing dataset. Such a zone was in a similar position with the average values of R^2, ranging from 3 to 8 neurons in the first hidden layer and from 4 to 6 in the second hidden layer.

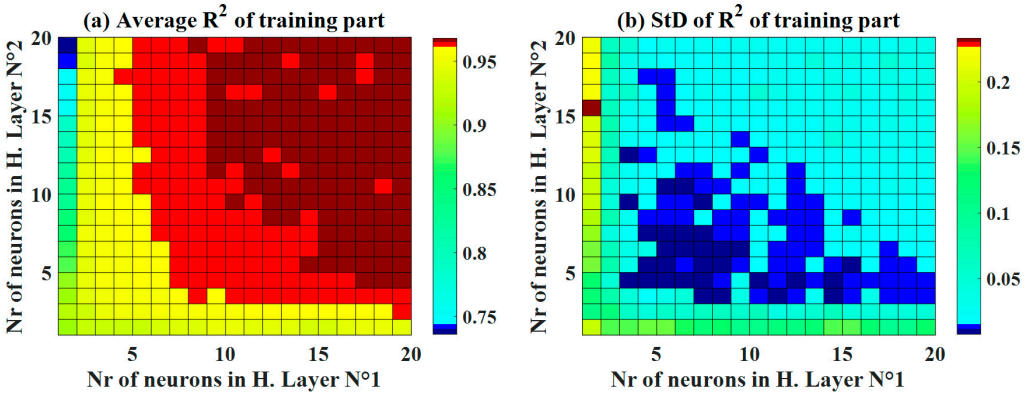

Figure 4. *Cont.*

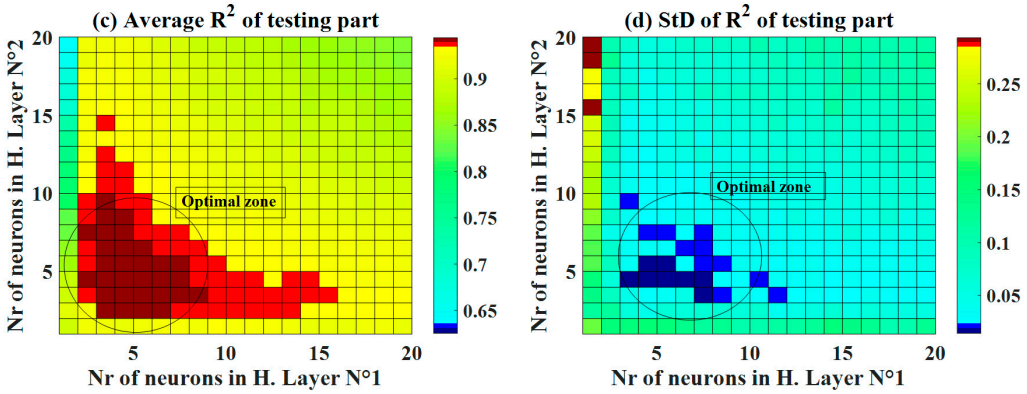

Figure 4. Maps of the performance indicator R^2 as a function of the number of neurons in hidden layers No. 1 and 2, for both the mean and standard deviation values over 1000 random samplings

Using RMSE, Figure 5 displays the average values of RMSE and the corresponding standard deviation for the training and testing datasets. Similar to the case of R^2, the better the accuracy of C-ANN increased when the number of neurons in the two hidden layers increased. The optimal zone of neurons was also determined with a moderate number of neurons (Figure 5c) for the testing dataset with respect to both the average RMSE values and the standard deviation. It is also noticed that for the training part, the lowest values of standard deviation were found around the C-ANN-[3–4–5–1] zone. Similar observations were found using the average values and standard deviation of MAE (Figure 6). It can be stated that an increase in the number of neurons in the hidden layers can improve the accuracy of the C-ANN for the training dataset, and the optimal architecture of the C-ANN was selected as C-ANN-[3–4–5–1] (Figure 7).

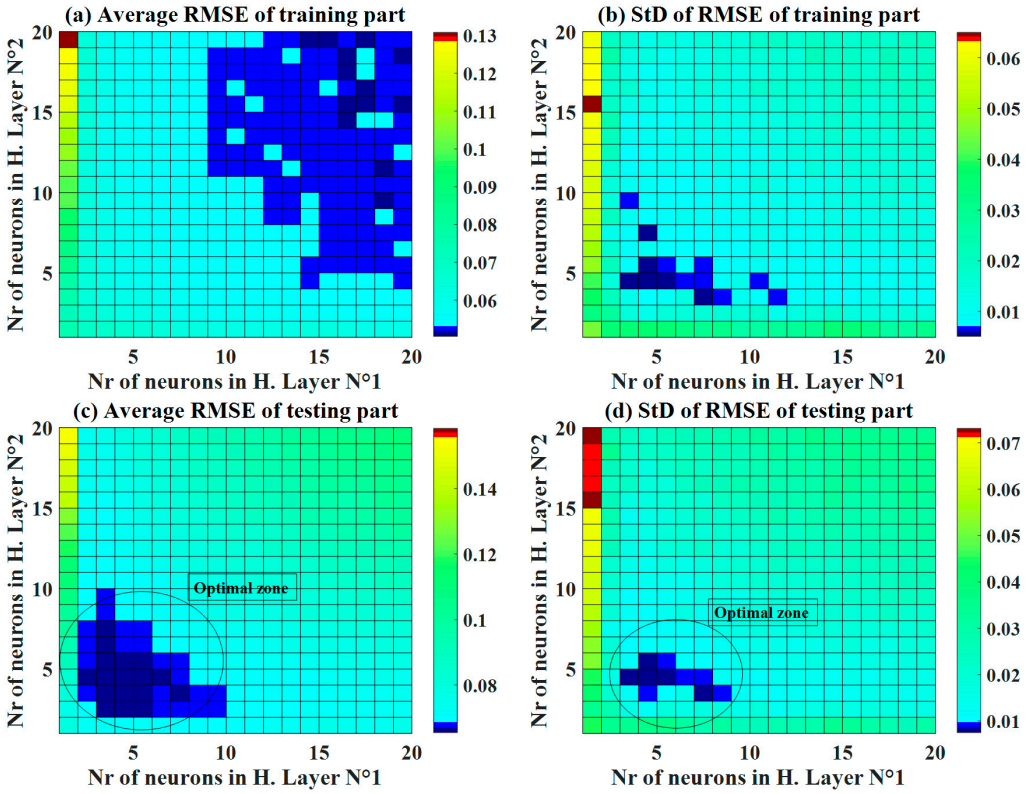

Figure 5. Maps of the performance indicator RMSE as a function of the number of neurons in hidden layers No. 1 and 2, for both the mean and standard deviation values over 1000 random samplings

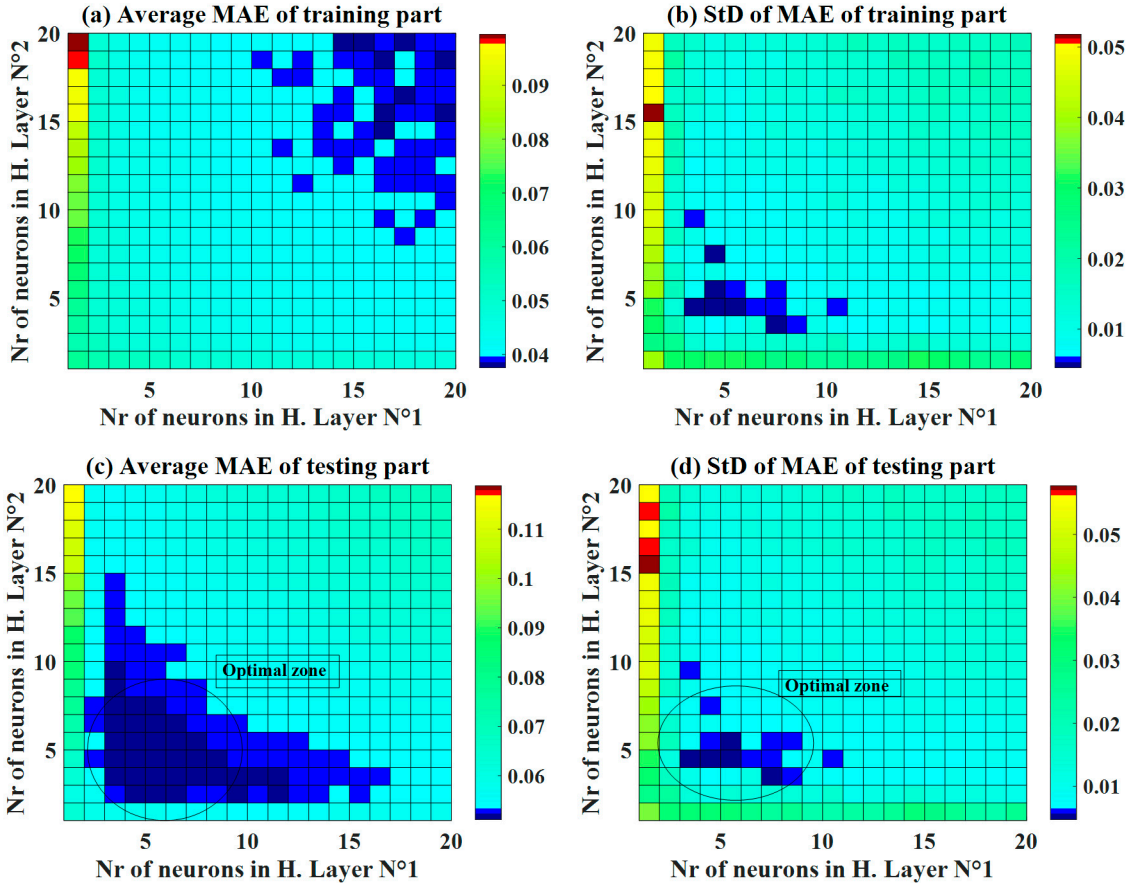

Figure 6. Maps of the performance indicator MAE as a function of the number of neurons in hidden layers No. 1 and 2, for both the mean and standard deviation value over 1000 random samplings (**a–d**).

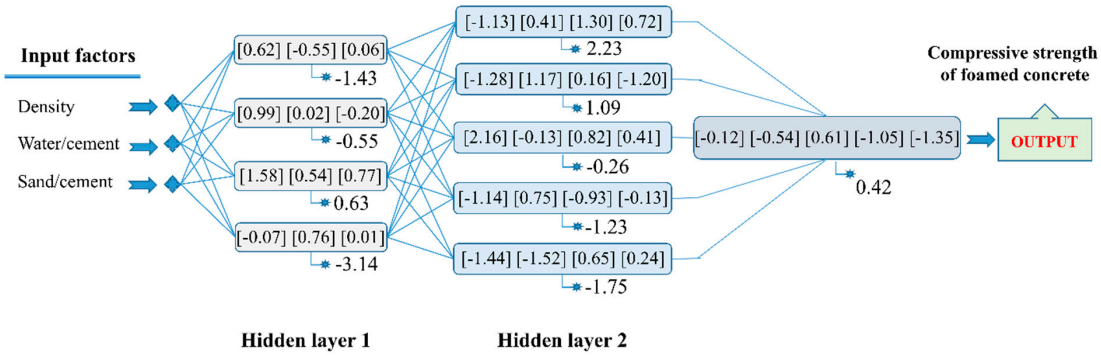

Figure 7. The architecture of the optimal C-ANN-[3–4–5–1] with weights (presented in [. . .]) and biases (presented along the stars).

4.3. Robustness of Optimal C-ANN Structure

The robustness of the optimal C-ANN structure of C-ANN-[3–4–5–1] was analyzed using MCS (Figure 8). From a statistical point of view, Figure 8 shows the distribution of the performance indicators over 1000 realizations using the optimal C-ANN architecture, whereas the statistical analysis is highlighted in Table 3. The values of the average and standard deviation of the R^2 values are given in Figure 8a and those of the RMSE and MAE are plotted in Figure 8b for the training and testing datasets.

It can be seen that the performance indicators of the training part is better than the testing one, which could avoid overfitting problems. While the curves of R^2, RMSE, and MAE were rather narrow, the curves of slope for the testing part were rather broad. In all the cases, the distributions of the results followed a Gaussian distribution but with different standard deviations. In addition, the values

of three levels of quantiles (Q25, Q50, and Q75) with the coefficient of variation are given in Table 3. As expected, the optimal architecture provided a high performance of prediction as well as a low value of coefficient of variation (CV). In terms of CV, the model also proved as a robust predictor. Values of CV of RMSE and MAE were approximately 10% due to the small mean values. In case of R^2 and slope, CVs were lower than 3.2%.

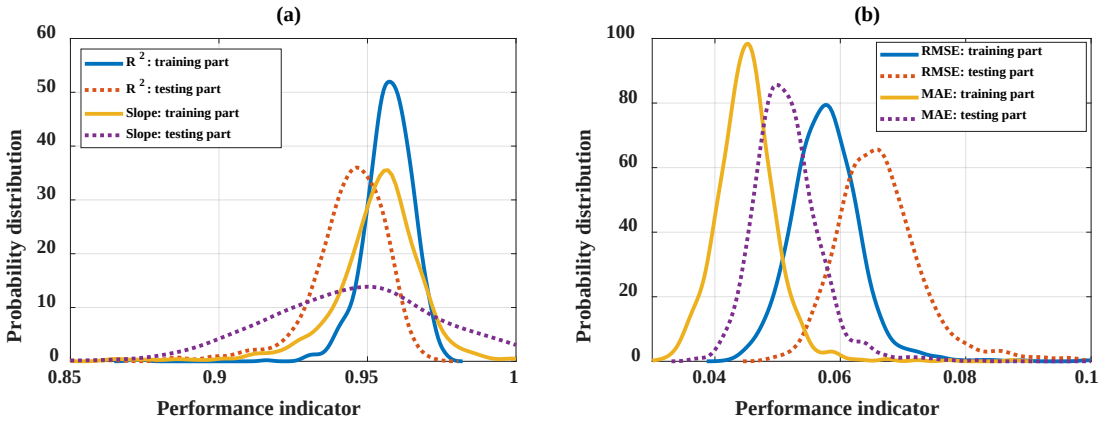

Figure 8. The distribution of performance indicators over 1000 runs using the optimal C-ANN architecture: (**a**) for R^2 and slope, (**b**) for RMSE and MAE (**a–b**).

Table 3. Statistical analysis of performance indicators over 1000 runs using the optimal C-ANN architecture.

Parameters	Training Part				Testing Part			
	R^2	Slope	RMSE	MAE	R^2	Slope	RMSE	MAE
Min	0.871	0.779	0.043	0.031	0.800	0.776	0.049	0.037
Q25	0.953	0.947	0.054	0.042	0.938	0.925	0.062	0.048
Q50	0.958	0.955	0.058	0.045	0.945	0.947	0.066	0.051
Q75	0.963	0.962	0.061	0.048	0.952	0.964	0.070	0.054
Max	0.976	1.026	0.109	0.088	0.972	1.027	0.140	0.114
Mean	0.957	0.953	0.058	0.045	0.943	0.945	0.067	0.052
SD*	0.009	0.019	0.006	0.005	0.015	0.031	0.008	0.006
CV (%)	0.907	1.987	9.880	10.874	1.594	3.267	11.718	10.785

SD* = standard deviation.

4.4. Interpretation of Relationship between of Inputs and Output Using PDP

In general, the use of PDP is effective in interpreting the relationships between the inputs and the predicted output [79]. As seen in Figure 9, all considered input variables affected the 28-days CS of FC; however, at different amplitudes. For instance, the CS of FC decreased when the water/cement ratio (W/C) and sand/cement ratio (S/C) increased, but it increased when dry density (D) increased. Thus, the water/cement ratio (W/C) and sand/cement ratio (S/C) had a negative effect, whereas dry density had a positive effect on the CS of FS. It is seen that the PDP investigation for each input could be approximated by a different fit (i.e., exponential, quadratic, and linear). Table 4 summarizes the overall values of the PDP investigation, including a classification of the influence of the level of inputs and the negative and positive effects of such input to the predicted output.

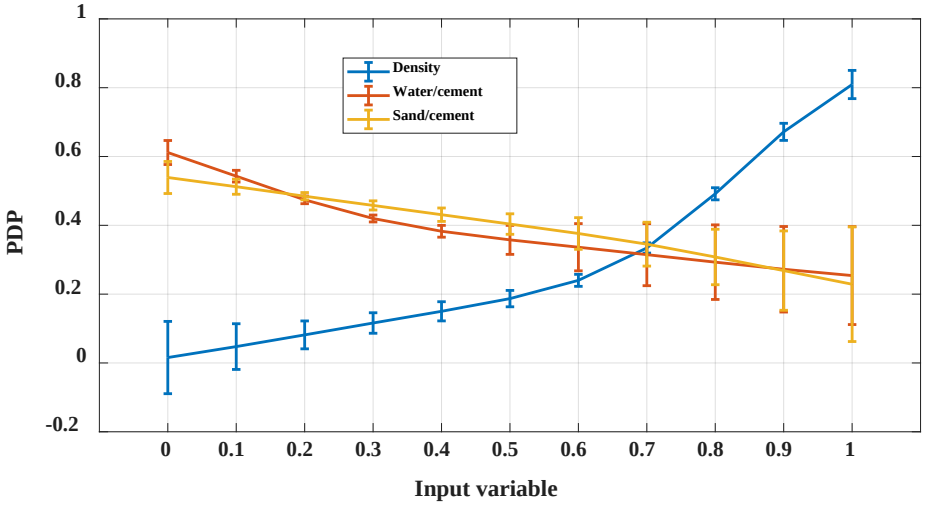

Figure 9. PDP curves in function of input variables.

Table 4. Analysis and interpretation of PDP curves.

Input	Fit	Equation Form	Effect	Nature of Correlation Effect	Rank
Density	Exponential	CS = 0.044* exp(2.967 D)	Positive	Nonlinear	1
W/C	Quadratic	CS = 0.31 W/C ^{2} - 0.64 W/C + 0.60	Negative	Nonlinear	3
S/C	Linear	CS = -0.3 S/C + 0.55	Negative	Linear	2

5. Discussion

A machine learning algorithm like C-ANN has been widely and effectively applied in different fields for solving a lot of real-world problems, including material sciences [80,81]. Although this approach is proved as a promising tool and technique for better performance of the model, the accuracy of this approach depends significantly on the selection of network structures [82–84]. In this study, a thorough investigation of ANN structures has been carried out for predicting the 28 days CS of FC, which is one of the most important mechanical properties of FC. In addition, it is well-known that the accuracy of the given machine learning algorithm greatly depends on the sampling strategy to construct the model [85,86]. Therefore, MCS was used in this study to fully analyze the capability of all the C-ANN structures, taking into account such variability of the input space in the training phase of the model. As a result, an accuracy map was given where an optimal structure was defined by statistical analysis of many criteria, such as the maximum average values of the R^2, RMSE, and MAE, as well as the minimum values of the standard deviation of R^2, RMSE, and MAE.

The investigation results showed that a good result could be obtained with simple machine learning algorithms like the C-ANN, as long as the structure and the parameters were well established. The optimization results of the C-ANN structure also showed that increasing the number of neurons in the hidden layers can enhance the accuracy of the C-ANN for the training dataset, and the optimal architecture of the C-ANN was selected as C-ANN-[3–4–5–1]. It is worth noticing that the maximum value of the R2 for the testing part, in this study, could reach an accuracy of R^2 = 0.972 (R = 0.986). This value is amongst the best accuracies reported in the literature, as compared with results in [25,47]. Similar observations with respect to criteria such as RMSE or MAE were also noticed and compared with previously published works, such as the RMSE = 1.808 [47] or 1.65 [25], but these studies used only 177 instances [25] or 150 samples [47].

In addition, it is also noticed that the performance of machine learning models such as C-ANN depends on the selection of input factors used in the datasets. Therefore, a sensitivity analysis should be carried out to (i) verify the performance of the C-ANN model on the choice of features in the input space and (ii) interpret the relationships between the input variables and the 28 days FC of CS. For this, such relationships were investigated thanks to PDP. In general, PDP analysis is given as the result of

one constructed machine learning model. Thus, the results are influenced by the accuracy of such model and it could vary in function of the random sampling strategies. Again, the PDP analysis in this study was taken as the average of 1000 reliable simulations and could be confident for further investigations. The results of this study are in agreement with the findings in the literature, which stated that the 28-days CS of FC increased exponentially with an increase in dry density (D) [23,47]. Besides, a previous study of Hoff [87] indicated that for a certain range of density, this relationship can be linear, as observed for the scaled density from 0 to 0.5 in this study. However, for the whole range of density, an exponential relationship is assumed. The positive effect of dry density (D) and cement content was confirmed and had a significant role in designing FC mixes [47]. Meanwhile, a negative effect on the CS of FC was confirmed to be associated with an increase in the water/cement ratio (W/C) and sand/cement ratio (S/C) [47]. Moreover, the water/cement ratio (W/C) is a controlling factor of the CS of FC [88], or, an appropriate content of water enhances the consistency and stability of FC, which increase the CS of FC [10,89].

6. Conclusion

Despite a number of studies on the prediction of the CS of FC using ML, the prediction performance could still benefit from more in-depth investigations. The current study showed a simple but efficient manner to use an ANN structure to predict the 28-days CS of FC. An optimal C-ANN-[3–4–5–1] was proposed, where the robustness was confirmed in the presence of a random dataset splitting over 1000 MCS. Statistical assessment of the results was derived to verify the reliability of predicted results and testify the convergence of the outcomes of C-ANN. A simple and optimal C-ANN structure was proven to produce comparative results with complex algorithms proposed in the literature, where the value of R^2 could reach $R^2 = 0.972$. A comprehensive interpretation of the results using PDP investigations was performed and derived several relationships, revealing the dependence of the 28-days CS of FC on the dry density (D), water/cement ratio (W/C), and sand/cement ratio (S/C). Overall, dry density (D) was found to be the most affecting factor, which had a significant role on the 28-days CS of FC. The results of the present study could facilitate and enhance the use of C-ANN in other civil engineering-related problems. Two perspectives can be envisioned: (i) gathering more data to cover larger ranges of input and output variables, and (ii) implementing optimization techniques to improve the accuracy of the C-ANN algorithm.

Author Contributions: Conceptualization, D.V.D., H.-B.L., T.-T.L. and B.T.P.; methodology, D.V.D. and B.T.P.; validation, H.-B.L. and B.T.P.; formal analysis, D.V.D., H.-L.T.V., T.-T.L.; investigation, H.-B.L. and H.-L.T.V.; data curation, H.-L.T.V and T.-T.L.; writing—original draft preparation, D.V.D., H.-B.L., T.-T.L. and B.T.P.; visualization, T.-T.L.; supervision, D.V.D. and H.-B.L.; project administration, D.V.D. and B.T.P. All authors have read and agreed to the published version of the manuscript.

Funding: This research received no external funding.

Conflicts of Interest: The authors declare no conflict of interest.

References

1. Ali, M.M. Evolution of concrete skyscrapers: From Ingalls to Jin mao. *J.Struct. Eng.* **2001**, *1*, 2–14.
2. Ali, M.M.; Moon, K.S. Advances in structural systems for tall buildings: Emerging developments for contemporary urban giants. *Buildings* **2018**, *8*, 104. [CrossRef]
3. Hilal, A.A.; Thom, N.; Dawson, A. The use of additives to enhance properties of pre-formed foamed concrete. *Int. J. Eng. Technol. Innov.* **2015**, *7*, 286–293. [CrossRef]
4. Sajedi, F.; Shafigh, P. High-strength lightweight concrete using leca, silica fume, and limestone. *Arab. J. Sci. Eng.* **2012**, *37*, 1885–1893. [CrossRef]
5. Topçu, İ.B.; Işıkdağ, B. Effect of expanded perlite aggregate on the properties of lightweight concrete. *J. Mater. Process. Technol.* **2008**, *204*, 34–38. [CrossRef]
6. Pan, Z.; Hiromi, F.; Wee, T. Preparation of high performance foamed concrete from cement, sand and mineral admixtures. *J.Wuhan Univ.Technol.* **2007**, *22*, 295–298. [CrossRef]

7. Ramamurthy, K.; Nambiar, E.K.; Ranjani, G.I.S. A classification of studies on properties of foam concrete. *Cem. Concr. Compos.* **2009**, *31*, 388–396. [CrossRef]
8. Panesar, D.K. Cellular concrete properties and the effect of synthetic and protein foaming agents. *Constr. Build. Mater.* **2013**, *44*, 575–584. [CrossRef]
9. Kiani, B.; Gandomi, A.H.; Sajedi, S.; Liang, R.Y. New formulation of compressive strength of preformed-foam cellular concrete: An evolutionary approach. *J. Mater. Civ. Eng.* **2016**, *28*, 04016092. [CrossRef]
10. Tam, C.T.; Lim, T.Y.; Sri Ravindrarajah, R.; Lee, S.L. Relationship between strength and volumetric composition of moist-cured cellular concrete. *Mag. Concr. Res.* **1987**, *39*, 12–18. [CrossRef]
11. Tikalsky, P.J.; Pospisil, J.; MacDonald, W. A method for assessment of the freeze–thaw resistance of preformed foam cellular concrete. *Cem. Concr. Res.* **2004**, *34*, 889–893. [CrossRef]
12. Jones, M.R.; McCarthy, A. Preliminary views on the potential of foamed concrete as a structural material. *Mag. Concr. Res.* **2005**, *57*, 21–31. [CrossRef]
13. Shi, X.; She, W.; Zhou, H.; Zhang, Y.; Shi, F.; Chen, W. Thermal upgrading of Hui-style vernacular dwellings in China using foam concrete. *Front. Archit. Res.* **2012**, *1*, 23–33. [CrossRef]
14. Sun, H.Y.; Gong, A.M.; Peng, Y.L.; Wang, X. The study of foamed concrete with polypropylene fiber and high volume fly ash. In *Proceedings of the Applied Mechanics and Materials*; Trans Tech Publ.: Stafa-Zurich, Switzerland, 2011; Volume 90, pp. 1039–1043.
15. Harith, I.K. Study on polyurethane foamed concrete for use in structural applications. *Case Stud. Constr. Mater.* **2018**, *8*, 79–86. [CrossRef]
16. Mounanga, P.; Gbongbon, W.; Poullain, P.; Turcry, P. Proportioning and characterization of lightweight concrete mixtures made with rigid polyurethane foam wastes. *Cem. Concr. Compos.* **2008**, *30*, 806–814. [CrossRef]
17. Koz\lowski, M.; Kadela, M.; Kukie\lka, A. Fracture energy of foamed concrete based on three-point bending test on notched beams. *Procedia Eng.* **2015**, *108*, 349–354. [CrossRef]
18. Sayadi, A.A.; Tapia, J.V.; Neitzert, T.R.; Clifton, G.C. Effects of expanded polystyrene (EPS) particles on fire resistance, thermal conductivity and compressive strength of foamed concrete. *Constr. Build. Mater.* **2016**, *112*, 716–724. [CrossRef]
19. Kearsley, E.P.; Wainwright, P.J. The effect of porosity on the strength of foamed concrete. *Cem. Concr. Res.* **2002**, *32*, 233–239. [CrossRef]
20. Yaseen, Z.M.; Deo, R.C.; Hilal, A.; Abd, A.M.; Bueno, L.C.; Salcedo-Sanz, S.; Nehdi, M.L. Predicting compressive strength of lightweight foamed concrete using extreme learning machine model. *Adv. Eng. Software* **2018**, *115*, 112–125. [CrossRef]
21. Asadzadeh, S.; Khoshbayan, S. Multi-objective optimization of influential factors on production process of foamed concrete using Box-Behnken approach. *Constr. Build. Mater.* **2018**, *170*, 101–110. [CrossRef]
22. Kockal, N.U.; Ozturan, T. Optimization of properties of fly ash aggregates for high-strength lightweight concrete production. *Mater. Des.* **2011**, *32*, 3586–3593. [CrossRef]
23. Bing, C.; Zhen, W.; Ning, L. Experimental research on properties of high-strength foamed concrete. *J. Mater. Civ. Eng.* **2011**, *24*, 113–118. [CrossRef]
24. Liu, M.Y.J.; Alengaram, U.J.; Jumaat, M.Z.; Mo, K.H. Evaluation of thermal conductivity, mechanical and transport properties of lightweight aggregate foamed geopolymer concrete. *Energy Build.* **2014**, *72*, 238–245. [CrossRef]
25. Nguyen, T.; Kashani, A.; Ngo, T.; Bordas, S. Deep neural network with high-order neuron for the prediction of foamed concrete strength. *Comput.-Aided Civ. Infrastruct. Eng.* **2019**, *34*, 316–332. [CrossRef]
26. Ashrafian, A.; Shokri, F.; Amiri, M.J.T.; Yaseen, Z.M.; Rezaie-Balf, M. Compressive strength of Foamed Cellular Lightweight Concrete simulation: New development of hybrid artificial intelligence model. *Constr. Build. Mater.* **2020**, *230*, 117048. [CrossRef]
27. Le, L.M.; Ly, H.B.; Pham, B.T.; Le, V.M.; Pham, T.A.; Nguyen, D.-H.; Tran, X.T.; Le, T.T. Hybrid Artificial Intelligence Approaches for Predicting Buckling Damage of Steel Columns Under Axial Compression. *Materials* **2019**, *12*, 1670. [CrossRef]
28. Ly, H.B.; Le, L.M.; Duong, H.T.; Nguyen, T.C.; Pham, T.A.; Le, T.T.; Le, V.M.; Nguyen-Ngoc, L.; Pham, B.T. Hybrid Artificial Intelligence Approaches for Predicting Critical Buckling Load of Structural Members under Compression Considering the Influence of Initial Geometric Imperfections. *Appl. Sci.* **2019**, *9*, 2258. [CrossRef]

29. Ly, H.B.; Le, T.T.; Le, L.M.; Tran, V.Q.; Le, V.M.; Vu, H.-L.T.; Nguyen, Q.H.; Pham, B.T. Development of Hybrid Machine Learning Models for Predicting the Critical Buckling Load of I-Shaped Cellular Beams. *Appl. Sci.* **2019**, *9*, 5458. [CrossRef]
30. Dao, D.V.; Trinh, S.H.; Ly, H.-B.; Pham, B.T. Prediction of Compressive Strength of Geopolymer Concrete Using Entirely Steel Slag Aggregates: Novel Hybrid Artificial Intelligence Approaches. *Appl. Sci.* **2019**, *9*, 1113. [CrossRef]
31. Dao, D.V.; Ly, H.B.; Trinh, S.H.; Le, T.-T.; Pham, B.T. Artificial Intelligence Approaches for Prediction of Compressive Strength of Geopolymer Concrete. *Materials* **2019**, *12*, 983. [CrossRef]
32. Ly, H.-B.; Pham, B.T.; Dao, D.V.; Le, V.M.; Le, L.M.; Le, T.-T. Improvement of ANFIS Model for Prediction of Compressive Strength of Manufactured Sand Concrete. *Appl. Sci.* **2019**, *9*, 3841. [CrossRef]
33. Qi, C.; Ly, H.-B.; Chen, Q.; Le, T.-T.; Le, V.M.; Pham, B.T. Flocculation-dewatering prediction of fine mineral tailings using a hybrid machine learning approach. *Chemosphere* **2019**, 125450. [CrossRef] [PubMed]
34. Pham, B.T.; Nguyen, M.D.; Dao, D.V.; Prakash, I.; Ly, H.-B.; Le, T.-T.; Ho, L.S.; Nguyen, K.T.; Ngo, T.Q.; Hoang, V.; et al. Development of artificial intelligence models for the prediction of Compression Coefficient of soil: An application of Monte Carlo sensitivity analysis. *Sci. Total Environ.* **2019**, *679*, 172–184. [CrossRef]
35. Pham, B.T.; Nguyen, M.D.; Ly, H.B.; Pham, T.A.; Hoang, V.; Van Le, H.; Le, T.T.; Nguyen, H.Q.; Bui, G.L. Development of Artificial Neural Networks for Prediction of Compression Coefficient of Soft Soil. In Proceedings of the CIGOS 2019, Innovation for Sustainable Infrastructure, Hanoi, Vietnam, 31 October 2020; pp. 1167–1172.
36. Yong, W.; Zhou, J.; Jahed Armaghani, D.; Tahir, M.M.; Tarinejad, R.; Pham, B.T.; Van Huynh, V. A new hybrid simulated annealing-based genetic programming technique to predict the ultimate bearing capacity of piles. *Eng. Comp.* **2020**, 1–17. [CrossRef]
37. Pham, B.T.; Tien Bui, D.; Pham, H.V.; Le, H.Q.; Prakash, I.; Dholakia, M.B. Landslide Hazard Assessment Using Random SubSpace Fuzzy Rules Based Classifier Ensemble and Probability Analysis of Rainfall Data: A Case Study at Mu Cang Chai District, Yen Bai Province (Viet Nam). *J. Indian Soc. Remote Sens.* **2017**, *45*, 673–683. [CrossRef]
38. Dou, J.; Yunus, A.P.; Xu, Y.; Zhu, Z.; Chen, C.-W.; Sahana, M.; Khosravi, K.; Yang, Y.; Pham, B.T. Torrential rainfall-triggered shallow landslide characteristics and susceptibility assessment using ensemble data-driven models in the Dongjiang Reservoir Watershed, China. *Nat. Hazards* **2019**, *97*, 579–609. [CrossRef]
39. Chang, K.-T.; Merghadi, A.; Yunus, A.P.; Pham, B.T.; Dou, J. Evaluating scale effects of topographic variables in landslide susceptibility models using GIS-based machine learning techniques. *Sci. Rep.* **2019**, *9*, 1–21. [CrossRef]
40. Dao, D.V.; Jaafari, A.; Bayat, M.; Mafi-Gholami, D.; Qi, C.; Moayedi, H.; Phong, T.V.; Ly, H.B.; Le, T.T.; Trinh, P.T. A spatially explicit deep learning neural network model for the prediction of landslide susceptibility. *Catena* **2020**, *188*, 104451. [CrossRef]
41. Khosravi, K.; Daggupati, P.; Alami, M.T.; Awadh, S.M.; Ghareb, M.I.; Panahi, M.; Pham, B.T.; Rezaie, F.; Qi, C.; Yaseen, Z.M. Meteorological data mining and hybrid data-intelligence models for reference evaporation simulation: A case study in Iraq. *Comput. Electron. Agric.* **2019**, *167*, 105041. [CrossRef]
42. Khosravi, K.; Barzegar, R.; Miraki, S.; Adamowski, J.; Daggupati, P.; Alizadeh, M.R.; Pham, B.T.; Alami, M.T. Stochastic Modeling of Groundwater Fluoride Contamination: Introducing Lazy Learners. *Groundwater* **2019**. [CrossRef]
43. Pham, B.T.; Prakash, I.; Khosravi, K.; Chapi, K.; Trinh, P.T.; Ngo, T.Q.; Hosseini, S.V.; Bui, D.T. A comparison of Support Vector Machines and Bayesian algorithms for landslide susceptibility modelling. *Geocarto Int.* **2019**, *34*, 1385–1407. [CrossRef]
44. Nguyen, V.T.; Tran, T.H.; Ha, N.A.; Ngo, V.L.; Nadhir, A.A.; Tran, V.P.; Duy Nguyen, H.; MA, M.; Amini, A.; Prakash, I. GIS Based Novel Hybrid Computational Intelligence Models for Mapping Landslide Susceptibility: A Case Study at Da Lat City, Vietnam. *Sustainability* **2019**, *11*, 7118. [CrossRef]
45. Pham, B.T.; Phong, T.V.; Nguyen, H.D.; Qi, C.; Al-Ansari, N.; Amini, A.; Ho, L.S.; Tuyen, T.T.; Yen, H.P.H.; Ly, H.-B.; et al. A Comparative Study of Kernel Logistic Regression, Radial Basis Function Classifier, Multinomial Naïve Bayes, and Logistic Model Tree for Flash Flood Susceptibility Mapping. *Water* **2020**, *12*, 239. [CrossRef]
46. Thai Pham, B.; Tien Bui, D.; Prakash, I. Landslide susceptibility modelling using different advanced decision trees methods. *Civil Eng. Environ. Syst.* **2018**, *35*, 139–157. [CrossRef]

47. Abd, A.M.; Abd, S.M. Modelling the strength of lightweight foamed concrete using support vector machine (SVM). *Case Studies in Construction Materials* **2017**, *6*, 8–15. [CrossRef]
48. Asteris, P.G.; Roussis, P.C.; Douvika, M.G. Feed-Forward Neural Network Prediction of the Mechanical Properties of Sandcrete Materials. *Sensors* **2017**, *17*, 1344. [CrossRef] [PubMed]
49. Asteris, P.G.; Kolovos, K.G.; Douvika, M.G.; Roinos, K. Prediction of self-compacting concrete strength using artificial neural networks. *Eur. J. Environ. Civ. Eng.* **2016**, *20*, s102–s122. [CrossRef]
50. Richard, A.O.; Ramli, M. Experimental production of sustainable lightweight foamed concrete. *J. Appl. Sci. Eng.* **2013**, 994–1005. [CrossRef]
51. Russell, S.J.; Norvig, P. *Artificial intelligence: A modern approach*, 3th ed.; Pearson Education Limited: Essex, England, 2009.
52. Adeli, H. Neural Networks in Civil Engineering: 1989–2000. *Comput.-Aided Civ. Infrastruct. Eng.* **2001**, *16*, 126–142. [CrossRef]
53. Sarir, P.; Shen, S.-L.; Wang, Z.-F.; Chen, J.; Horpibulsuk, S.; Pham, B.T. Optimum model for bearing capacity of concrete-steel columns with AI technology via incorporating the algorithms of IWO and ABC. *Eng. Comput.* **2019**. [CrossRef]
54. Pham, B.T.; Nguyen, M.D.; Bui, K.-T.T.; Prakash, I.; Chapi, K.; Bui, D.T. A novel artificial intelligence approach based on Multi-layer Perceptron Neural Network and Biogeography-based Optimization for predicting coefficient of consolidation of soil. *Catena* **2019**, *173*, 302–311. [CrossRef]
55. Le, T.T.; Pham, B.T.; Ly, H.B.; Shirzadi, A.; Le, L.M. Development of 48-hour Precipitation Forecasting Model using Nonlinear Autoregressive Neural Network. In Proceedings of the CIGOS 2019, Innovation for Sustainable Infrastructure, Hanoi, Vietnam, 31 October 2020; pp. 1191–1196.
56. Pham, B.T.; Tien Bui, D.; Prakash, I.; Dholakia, M.B. Hybrid integration of Multilayer Perceptron Neural Networks and machine learning ensembles for landslide susceptibility assessment at Himalayan area (India) using GIS. *Catena* **2017**, *149*, 52–63. [CrossRef]
57. McCulloch, W.S.; Pitts, W. A logical calculus of the ideas immanent in nervous activity. *Bull. Math. Biophys.* **1943**, *5*, 115–133. [CrossRef]
58. Siddique, N.; Adeli, H. *Computational Intelligence: Synergies of Fuzzy Logic, Neural Networks and Evolutionary Computing*; John Wiley & Sons: West Sussex, UK, 2013.
59. Nehdi, M.; Djebbar, Y.; Khan, A. Neural network model for preformed-foam cellular concrete. *Mater. J.* **2001**, *98*, 402–409.
60. Paulson, A.J.; Prabhavathy, R.A.; Rekh, S.; Brindha, E. Application of neural network for prediction of compressive strength of silica fume concrete. *Int. J. Civ. Eng. Technol.* **2019**, *10*, 1859–1867.
61. Ly, H.B.; Monteiro, E.; Le, T.T.; Le, V.M.; Dal, M.; Regnier, G.; Pham, B.T. Prediction and Sensitivity Analysis of Bubble Dissolution Time in 3D Selective Laser Sintering Using Ensemble Decision Trees. *Materials* **2019**, *12*, 1544. [CrossRef]
62. Ly, H.B.; Le, L.M.; Phi, L.V.; Phan, V.H.; Tran, V.Q.; Pham, B.T.; Le, T.T.; Derrible, S. Development of an AI Model to Measure Traffic Air Pollution from Multisensor and Weather Data. *Sensors* **2019**, *19*, 4941. [CrossRef]
63. Nguyen, H.-L.; Le, T.-H.; Pham, C.-T.; Le, T.-T.; Ho, L.S.; Le, V.M.; Pham, B.T.; Ly, H.-B. Development of Hybrid Artificial Intelligence Approaches and a Support Vector Machine Algorithm for Predicting the Marshall Parameters of Stone Matrix Asphalt. *Appl. Sci.* **2019**, *9*, 3172. [CrossRef]
64. Dao, D.V.; Adeli, H.; Ly, H.B.; Le, L.M.; Le, V.M.; Le, T.T.; Pham, B.T. A Sensitivity and Robustness Analysis of GPR and ANN for High-Performance Concrete Compressive Strength Prediction Using a Monte Carlo Simulation. *Sustainability* **2020**, *12*, 830. [CrossRef]
65. Pham, B.T.; Le, L.M.; Le, T.-T.; Bui, K.-T.T.; Le, V.M.; Ly, H.-B.; Prakash, I. Development of advanced artificial intelligence models for daily rainfall prediction. *Atmos. Res.* **2020**, *237*, 104845. [CrossRef]
66. Soize, C. *Stochastic Models of Uncertainties in Computational Mechanics*; Christian, P.dS., Ed.; Amer Society of Civil Engineers: Reston, VA, USA, 2012; ISBN 978-0-7844-1223-7.
67. Nguyen, H.-L.; Pham, B.T.; Son, L.H.; Thang, N.T.; Ly, H.-B.; Le, T.-T.; Ho, L.S.; Le, T.-H.; Tien Bui, D. Adaptive Network Based Fuzzy Inference System with Meta-Heuristic Optimizations for International Roughness Index Prediction. *Appl. Sci.* **2019**, *9*, 4715. [CrossRef]
68. Guilleminot, J.; Dolbow, J.E. Data-driven enhancement of fracture paths in random composites. *Mech. Res. Commun.* **2020**, *103*, 103443. [CrossRef]

69. Wang, H.; Guilleminot, J.; Soize, C. Modeling uncertainties in molecular dynamics simulations using a stochastic reduced-order basis. *Comput. Meth. Appl. Mech. Eng.* **2019**, *354*, 37–55. [CrossRef]
70. Ly, H.-B.; Desceliers, C.; Le, L.M.; Le, T.-T.; Pham, B.T.; Nguyen-Ngoc, L.; Doan, V.T.; Le, M. Quantification of Uncertainties on the Critical Buckling Load of Columns under Axial Compression with Uncertain Random Materials. *Materials* **2019**, *12*, 1828. [CrossRef] [PubMed]
71. Soize, C. *Uncertainty Quantification: An Accelerated Course with Advanced Applications in Computational Engineering*; Interdisciplinary Applied Mathematics; Springer International Publishing: Berlin, Germany, 2017; ISBN 978-3-319-54338-3.
72. Cunha, A.; Nasser, R.; Sampaio, R.; Lopes, H.; Breitman, K. Uncertainty quantification through the Monte Carlo method in a cloud computing setting. *Comput. Phys. Commu* **2014**, *185*, 1355–1363. [CrossRef]
73. Le, T.T.; Guilleminot, J.; Soize, C. Stochastic continuum modeling of random interphases from atomistic simulations. Application to a polymer nanocomposite. *Comput. Meth. Appl. Mech. Eng.* **2016**, *303*, 430–449. [CrossRef]
74. Soize, C.; Desceliers, C.; Guilleminot, J.; Le, T.T.; Nguyen, M.T.; Perrin, G.; Allain, J.M.; Gharbi, H.; Duhamel, D.; Funfschilling, C. Stochastic representations and statistical inverse identification for uncertainty quantification in computational mechanics. In Proceedings of the 1st ECCOMAS Thematic International Conference on Uncertainty Quantification in Computational Sciences and Engineering, The Island of Crete, Greece, 30 May 2015; pp. 1–26.
75. Mordechai, S. *Applications of Monte Carlo Method in Science and Engineering*; IntechoOpen: London, UK, 2011; ISBN 978-953-307-691-1.
76. Guilleminot, J.; Soize, C. Generalized stochastic approach for constitutive equation in linear elasticity: A random matrix model. *Int. J. Numer. Methods Eng.* **2012**, *90*, 613–635. [CrossRef]
77. Guilleminot, J.; Le, T.T.; Soize, C. Stochastic framework for modeling the linear apparent behavior of complex materials: Application to random porous materials with interphases. *Acta Mech. Sin.* **2013**, *29*, 773–782. [CrossRef]
78. Staber, B.; Guilleminot, J.; Soize, C.; Michopoulos, J.; Iliopoulos, A. Stochastic modeling and identification of a hyperelastic constitutive model for laminated composites. *Comput. Meth. Appl. Mech. Eng.* **2019**, *347*, 425–444. [CrossRef]
79. Goldstein, A.; Kapelner, A.; Bleich, J.; Pitkin, E. Peeking inside the black box: Visualizing statistical learning with plots of individual conditional expectation. *J. Comput. Graph. Stat.* **2015**, *24*, 44–65. [CrossRef]
80. Prasad, B.R.; Eskandari, H.; Reddy, B.V. Prediction of compressive strength of SCC and HPC with high volume fly ash using ANN. *Constr. Build. Mater.* **2009**, *23*, 117–128. [CrossRef]
81. Eskandari-Naddaf, H.; Kazemi, R. ANN prediction of cement mortar compressive strength, influence of cement strength class. *Constr. Build. Mater.* **2017**, *138*, 1–11. [CrossRef]
82. Mazon, A.J.; Zamora, I.; Gracia, J.; Sagastabeutia, K.J.; Saenz, J.R. Selecting ANN structures to find transmission faults. *IEEE Computer Applications in Power* **2001**, *14*, 44–48. [CrossRef]
83. Gracia, J.; Mazon, A.J.; Zamora, I. Best ANN structures for fault location in single-and double-circuit transmission lines. *IEEE Trans. Power Delivery* **2005**, *20*, 2389–2395. [CrossRef]
84. Baczyński, D.; Parol, M. Influence of artificial neural network structure on quality of short-term electric energy consumption forecast. *IEE Gener. Transm. Distrib.* **2004**, *151*, 241–245. [CrossRef]
85. Perry, G.L.; Dickson, M.E. Using Machine Learning to Predict Geomorphic Disturbance: The Effects of Sample Size, Sample Prevalence, and Sampling Strategy. *J. Geophys. Res. Earth Surf.* **2018**, *123*, 2954–2970. [CrossRef]
86. L'heureux, A.; Grolinger, K.; Elyamany, H.F.; Capretz, M.A. Machine learning with big data: Challenges and approaches. *IEEE Access* **2017**, *5*, 7776–7797. [CrossRef]
87. Hoff, G.C. Porosity-strength considerations for cellular concrete. *Cem. Concr. Res.* **1972**, *2*, 91–100. [CrossRef]
88. Amran, Y.M.; Farzadnia, N.; Ali, A.A. Properties and applications of foamed concrete; a review. *Constr. Build. Mater.* **2015**, *101*, 990–1005. [CrossRef]
89. De Rose, L.; Morris, J. *The Influence of Mix Design on the Properties of Microcellular Concrete*; Thomas Telford: London, UK, 1999.